Send Orders for Reprints to reprints@benthamscience.ae

The Open Medical Imaging Journal, **2015,** *9,* **1-8**

Open Access

Single-shot Multi-slice T1 Mapping at High Spatial Resolution – Inversion-Recovery FLASH with Radial Undersampling and Iterative Reconstruction

Xiaoqing Wang*, Volkert Roeloffs, K. Dietmar Merboldt, Dirk Voit, Sebastian Schätz, Jens Frahm

Biomedizinische NMR Forschungs GmbH am Max-Planck-Institut für biophysikalische Chemie, 37070 Göttingen, Germany

Abstract: *Purpose:* To develop a method for T1 mapping at high spatial resolution and for multiple slices.

Methods: The proposed method emerges as a single-shot inversion-recovery experiment which covers the entire spin-lattice relaxation process by serial acquisitions of highly undersampled radial FLASH images, either in single-slice or multi-slice mode. Serial image reconstructions are performed in time-reversed order and first involve regularized nonlinear inversion (NLINV) to estimate optimum coil sensitivity profiles. Subsequently, the coil profiles are fixed for the calculation of differently T1-weighted frames and the resulting linear inverse problem is solved by a conjugate gradient (CG) technique. T1 values are obtained by pixelwise fitting with a Deichmann correction modified for multi-slice applications.

Results: T1 accuracy was validated for a reference phantom. For human brain, T1 maps were obtained at 0.5 mm resolution for single-slice acquisitions and at 0.75 mm resolution for up to 5 simultaneous slices (5 mm thickness). Corresponding T1 maps of the liver were acquired at 1 mm and 1.5 mm resolution, respectively. All T1 values were in agreement with literature data.

Conclusion: Inversion-recovery sequences with highly undersampled radial FLASH images and NLINV/CG reconstruction allow for fast, robust and accurate T1 mapping at high spatial resolution and for multiple slices.

Keywords: Nonlinear inverse reconstruction, real-time MRI, spin-lattice relaxation, T1 contrast, T1 mapping.

INTRODUCTION

Rapid mapping of the spin-lattice relaxation process with quantitative evaluations of T1 relaxation times is widely used in clinical MRI. Initial studies focused on the human brain and combined a leading inversion pulse with a serial image acquisition scheme termed snapshot FLASH [1]. These early applications used Cartesian encoding and offered only limited spatiotemporal resolution. Since then the concept has been broadened to variable readout modules based on echo-planar imaging [2] or steady-state free precession imaging [3] and extended to various applications even including myocardial T1 quantification during breath hold [4]. The actual determination of T1 values has been improved by advanced fitting routines which correct for the disturbance of the native relaxation recovery by repetitive low-flip angle excitations [5, 6], while recent model-based approaches attempt to calculate T1 maps directly from raw data, e.g. see [7].

Here we propose an extension of the original inversion-recovery (IR) snapshot FLASH method which takes advantage of highly undersampled radial FLASH acquisitions and iterative image reconstruction. The approach covers the spin-lattice relaxation process after (nonselective) inversion of the longitudinal magnetization by a series of images with user-selectable choices of spatial and temporal resolution. It allows for both single-slice and simultaneous multi-slice applications. A preliminary account of this work has been given in abstract form [8].

The iterative reconstruction process benefits from a joint estimation of the actual image and its corresponding coil sensitivity profiles by regularized nonlinear inversion (NLINV) as previously introduced for real-time MRI [9-12]. It exploits the similarity of successive frames during the spin-lattice relaxation process by regularization with respect to a neighboring frame. Together with the acquisition of 5 complementary sets of spokes for successive frames, this regularization considerably enhances the usable degree of undersampling similar to temporal regularization for dynamic imaging [10]. The present study describes the specific acquisition and reconstruction method developed for inversion-recovery T1 mapping, validates the T1 determination with use of an experimental phantom and summarizes high-resolution data for various human tissues in applications to the brain and abdomen.

*Address correspondence to this author at the Biomedizinische NMR Forschungs GmbH am Max-Planck-Institut für biophysikalische Chemie, 37070 Göttingen, Germany; Tel: (+49) 551-201-1720; Fax: (+49) 551-201-1307; E-mail: xwang1@gwdg.de

1874-3471/15

METHODS

Inversion-Recovery FLASH MRI with Radial Undersampling

The proposed method is based on a single-shot IR experiment that maps a single T1 relaxation process in real time by serial imaging. It comprises an initial IR module which consists of a nonselective adiabatic 180° radiofrequency (RF) pulse and a spoiler gradient and is followed by a serial acquisition of highly undersampled radial FLASH images that monitor the T1 relaxation recovery with complementary sets of spokes each covering 360°. Typically, 5 sequential frames of the same slice were acquired with spatially distinct radial spokes which interleave spokes of preceding sets as previously described [13].

Multi-slice versions at reduced temporal sampling density are accomplished in a sequential manner, i.e. by sequentially acquiring full frames of individual slices rather than by interleaving single spokes. For single-slice applications, it is also possible to replace the FLASH sequence by a refocused FLASH or even fully-balanced SSFP acquisition as proposed by Scheffler and Hennig [3].

Image reconstructions are first based on NLINV as originally developed for parallel MRI [9] and more recently extended to real-time MRI at high temporal resolution [10]. These studies provide all necessary mathematical details. For T1 mapping, the joint estimation of images and coil sensitivities was performed in reverse chronologic order starting with the last frames of the relaxation process close to full recovery and proceeding toward the initial inversion. Because this strategy starts with only very mild changes from frame to frame, it easily achieves high-quality reconstructions of image and coil profiles. In fact, the NLINV reconstruction was applied for only the 10 last frames corresponding to 2 times 5 frames with complementary radial encodings. Subsequently, the optimized coil sensitivities were fixed and used for the reconstruction of the entire dataset in order to obtain quantitatively comparable frames for the complete IR time course. This strategy reduces the computational task to a linear inverse problem similar to a SENSE-like reconstruction [14], which was then solved by an iteratively regularized conjugate gradient (CG) method. Phantom and brain studies at submillimeter resolution employed 7 steps of the iteratively regularized Gauss-Newton method used for NLINV, compare (9,10) for technical details, and 7 iterations of the CG reconstruction which employed a maximum of 250 internal steps. Both iterative optimizations used regularization parameters that were divided by a factor of 2 for each iteration. Abdominal T1 mapping at slightly lower resolution relied on 6 Newton steps for NLINV and 6 CG iterations.

Time-reversed NLINV/CG reconstructions as well as T1 calculations (see below) were performed offline, while online monitoring was accomplished by standard NLINV reconstructions as routinely used in our lab for real-time MRI, for implementation and application details see [11, 12].

Quantitative T1 Analysis

Quantitative analyses of single-slice and multi-slice IR FLASH experiments involved a pixel-by-pixel determination of flip angle, proton density and T1 maps. The disturbance of the T1 relaxation process by continuous RF excitations with flip angle α has previously been described by Deichmann *et al.* [5].

$$M(t) = M_0^* - (M_0^* - M_{ini}) \exp(-t / T1^*) \quad (1)$$

With M_0^* the steady-state magnetization and M_{ini} the initial magnetization. Assuming TR << T1*,T1, the desired T1 value can then be calculated by

$$T1 = T1^*((M_0^* - M_{ini}) / M_0^* - 1) \quad (2)$$

As shown in Fig. (**1**) this study extended the single-slice method to a sequential multi-slice acquisition. In the latter case the IR time course interleaves the aforementioned T1* relaxation process with periods of true T1 relaxation which prevails during the recording of images from neighboring slices. These dynamics have been taken into account in close analogy to the treatment of a similar multi-slice situation for a spinlock sequence [15]. While the T1* regime is governed by Eq. (1), the longitudinal relaxation during the RF-free regime follows

$$M(t) = M_0 - (M_0 - M_{ini}) \exp(-t / T1) \quad (3)$$

with M_0 the equilibrium magnetization. The combination of both processes yields an explicit expression for the magnetization of one slice after a total number of j RF excitations. For the present implementation the j low-flip angle pulses correspond to the acquisition of $l = \lfloor j / (n_{sp} \cdot n_{sl}) \rfloor$ frames with n_{sp} radial spokes each covering n_{sl} slices. The resulting longitudinal magnetization reads

$$M_{l,k} = M_0^* - \left[M_0^* - \left(\beta \frac{1-\gamma^l}{1-\gamma} + \gamma^l M_{ini}\right)\right] e^{-\frac{kTR}{T1^*}} \quad (4)$$

$$\beta = M_0 \left(1 - e^{-\frac{n_{sp}(n_{sl}-1)TR}{T1}}\right)$$

$$+M_0^* e^{-\frac{n_{sp}(n_{sl}-1)TR}{T1}} \left(1 - e^{-\frac{n_{sp}TR}{T1^*}}\right)$$

$$\gamma = e^{-n_{sp}TR\left[\frac{n_{sl}-1}{T1}+\frac{1}{T1^*}\right]}$$

with k = j mod n_{sp}. The expression again yields a mono-exponential decay, while the initial magnetization M_{ini} depends on the slice of interest as the inversion time slightly varies for individual slices. A pixelwise estimation of the parameters M_0, M_0^* and T1* was achieved by minimizing the cost function $\sum_t \|M_t(M_0, M_0^*, T1^*) - y_t\|_2^2$ with t the time index for each frame and y_t the corresponding signal intensity. Numerical computations employed a Levenberg-Marquardt algorithm in MATLAB R2013a (MathWorks, Natick, MA) and successful minimization was defined by reaching a maximum number of 3000 iterations, a relative change in the norm of the parameter update of less than 10^{-4}, or a stepwise relative difference for the objective function value of less than 10^{-7}.

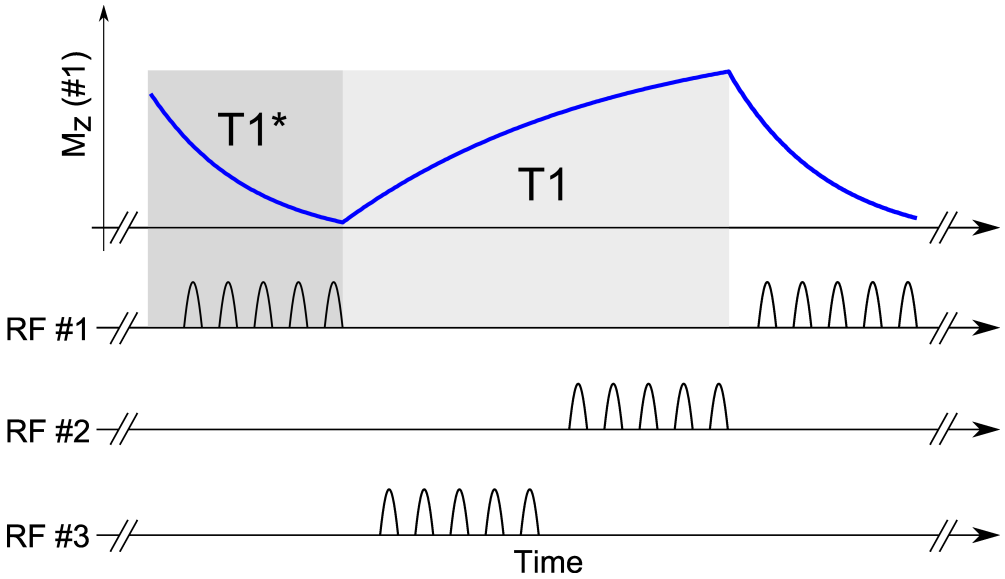

Fig. (1). Schematic representation of a small part of the dynamic inversion-recovery MRI signal for sequential 3-slice T1 mapping. During image formation the longitudinal magnetization M_z of slice #1 is governed by T1* due to repetitive low-flip angle RF excitations, while acquisitions of neighboring sections lead to periods of true T1 relaxation.

Table 1. Acquisition parameters for single-slice and multi-slice T1 mapping.

	Phantom/Head		Abdomen	
	Single Slice	**Multiple Slices**	**Single Slice**	**Multiple Slices**
Field-of-view / mm^2	192 × 192	192 × 192	320 × 320	320 × 320
Image matrix size	384 × 384	256 × 256	320 × 320	212 × 212
Resolution / mm^2	0.5 × 0.5	0.75 × 0.75	1.0 × 1.0	1.5 × 1.5
Thickness / mm	5	5	8	8
Repetition time / ms	3.37	2.64	2.25	1.93
Echo time / ms	2.25	1.76	1.47	1.25
Bandwidth / Hz $pixel^{-1}$	720	1090	1420	1970
Flip angle / degree	4	4	4	4
Spokes per frame	19	15	15	11
Time per frame / ms	64.0	39.6	33.8	21.2

Subjects and MRI

A total of 12 young volunteers (6 male, 6 female, age range 25.4 ± 3.7 years) without known illness were recruited for studies during technical development as well as for preliminary testing and final acquisitions. Written informed consent, according to the recommendations of the local ethics committee, was obtained from all subjects prior to MRI.

All studies were performed at 3T (Magnetom Prisma, Siemens Healthcare, Erlangen, Germany). Phantom and brain studies employed the standard 64-channel head coil, while abdominal scans relied on an 18-element thorax coil in conjunction with 18 elements of the spine coil. The outcome of the sequence optimization and modified reconstruction process led to single-slice and multi-slice protocols at two different resolutions for brain and abdominal T1 mapping. The corresponding experimental parameters are summarized in Table **1**. Abdominal measurements were performed during a brief breath hold.

RESULTS

(Fig. (**2**)) depicts proton density and T1 maps for a T1 reference phantom. The results were obtained for a single-slice acquisition at 0.5 mm resolution as well as for a 3-slice and 5-slice acquisition at 0.75 mm resolution. In all cases the maps correspond to the same section. Visual inspection reveals almost identical image quality and color-coded T1 values apart from a slightly enhanced noise level for 5-slice acquisitions. Corresponding single-pixel intensity time

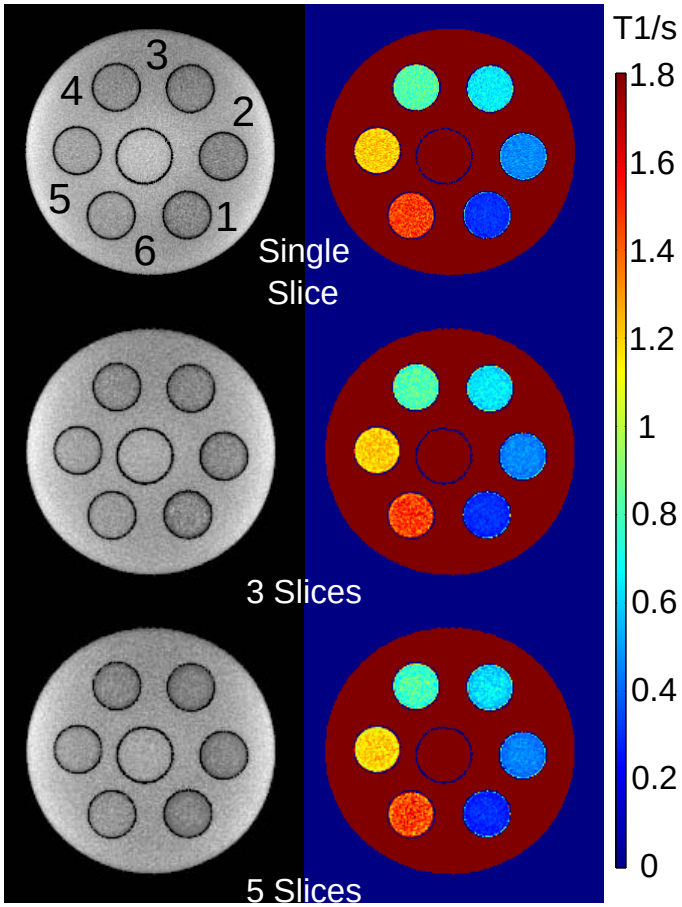

Fig. (2). Single-shot proton density and T1 maps obtained for a T1 reference phantom. (Top) Single-slice acquisition at 0.5 mm in-plane resolution, (middle) 3-slice and (bottom) 5-slice acquisition at 0.75 mm resolution (same section). For experimental details see Table **1**, numerical results for tubes 1 to 6 are given in Table **2**.

courses and fitting results are shown in Fig. (**3**) for three selected tubes with T1 values of 0.33 s, 0.68 s and 1.25 s (tubes 1, 3 and 5 in Fig. (**2**)). The numerical results summarized in Table **2** reveal accurate T1 determinations for both small and large T1 values when compared to a reference measurement using an IR spin-echo MRI sequence at long TR (7.2 s). Multi-slice acquisitions showed a mild tendency toward lower T1 relaxation times with increasing number of sections, while all values remained within one standard deviation.

In close analogy to the phantom data, Fig. (**4**) shows proton density and T1 maps for a single-slice (0.5 mm resolution), 3-slice and 5-slice acquisition (0.75 mm, same selected section) of the human brain. Again, apart from minor increases in the noise level for larger numbers of slices, all maps are of similar quality. This impression is confirmed by the numerical results in Table **3** for brain (frontal and parietal white and gray matter), liver, and kidney (cortex and medulla). Because a comprehensive determination of *in vivo* data for various tissues is outside the scope of this work, the present results are only compared to some most recent literature findings [16-18]. As it turns out all T1 values are close to published data. Finally, Fig. (**5**) shows all simultaneously acquired T1 maps of a transverse 5-slice acquisition of the liver at 1.5 mm resolution.

DISCUSSION

The combination of a conventional IR snapshot FLASH sequence with pronounced radial undersampling and iterative NLINV/CG image reconstruction allows for robust and efficient single-shot T1 mapping at high spatial resolution and for up to 5 simultaneous slices. Phantom studies confirm the excellent T1 accuracy achievable by a modified Deichmann correction for fitting sequential multi-slice acquisitions. Preliminary *in vivo* applications to human brain, liver and kidney are in agreement with literature values.

To the best of our knowledge this is the first method for single-shot multi-slice T1 mapping. Although a number of approaches have been described using undersampled radial acquisition schemes in conjunction with sliding-window and parallel imaging reconstructions [19-21], they only allow for single-slice applications. Moreover, respective studies of a phantom or human brain resulted in much lower spatial resolution of $1 \times 1 \times 8$ mm^3 = 8 mm^3 [19], $1.8 \times 1.8 \times 5$ mm^3 = 16.2 mm^3 [20] and $1.56 \times 1.56 \times 10$ mm^3 = 24.3 mm^3 [21] than achieved here for T1 mapping at voxel sizes of $0.5 \times 0.5 \times 5$ mm^3 = 1.25 mm^3 (single-slice) and $0.75 \times 0.75 \times 5$ mm^3 = 2.81 mm^3 (multi-slice). In comparison to model-based analyses of single-shot IR experiments, e.g. see [7], the proposed method is simple, mathematically robust and relatively

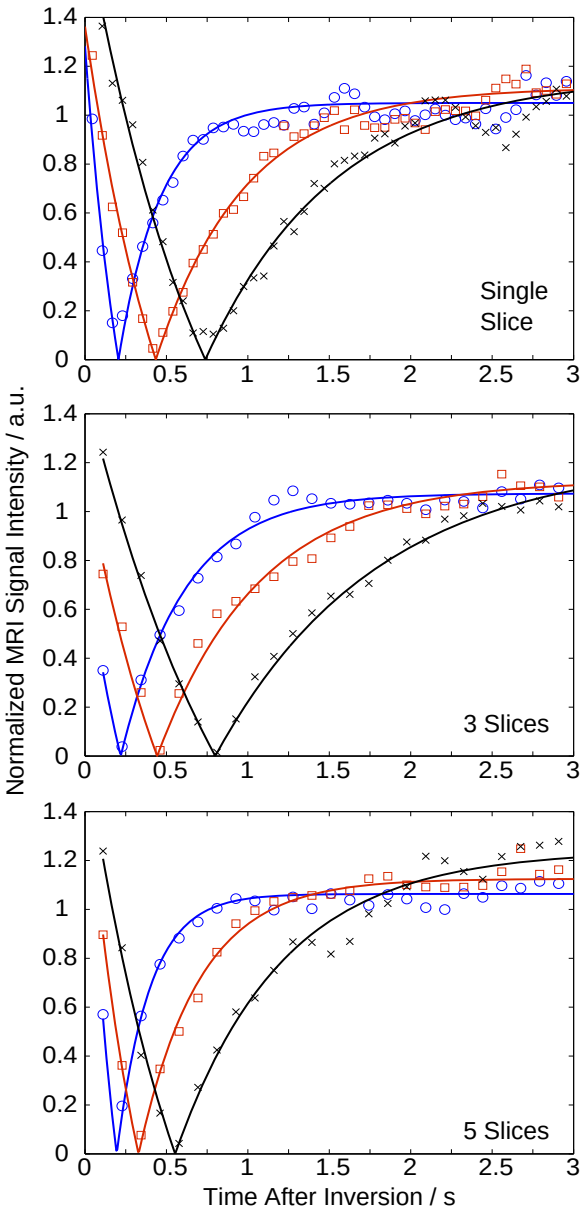

Fig. (3). Normalized MRI signal intensity time courses and respective fitting results for single pixels of the T1 reference phantom (tubes 1, 3 and 5 in Fig. (**2**) with T1 = 0.33 s (blue), 0.68 s (red), and 1.25 s (black). (Top) Single-slice acquisition at 0.5 mm resolution, (middle) 3-slice and (bottom) 5-slice acquisition at 0.75 mm resolution (same section).

Table 2. T1 relaxation times of a reference phantom obtained by single-slice and multi-slice T1 mapping.

ROI[1]	1 Slice	3 Slices	5 Slices	SE-MRI[2]
1	0.32 ± 0.03	0.31 ± 0.03	0.30 ± 0.03	0.33 ± 0.01
2	0.48 ± 0.04	0.46 ± 0.04	0.46 ± 0.04	0.50 ± 0.01
3	0.66 ± 0.06	0.65 ± 0.05	0.64 ± 0.06	0.68 ± 0.01
4	0.83 ± 0.07	0.82 ± 0.06	0.80 ± 0.07	0.86 ± 0.01
5	1.22 ± 0.07	1.22 ± 0.06	1.20 ± 0.07	1.25 ± 0.01
6	1.49 ± 0.09	1.48 ± 0.08	1.47 ± 0.10	1.50 ± 0.01

All values (mean ± SD) are given in s. Multi-slice data refer to the same section. [1]Region-of-interest as indicated in Fig. (**2**). [2]Reference data obtained by a long-TR (7.2 s) inversion-recovery spin-echo MRI sequence.

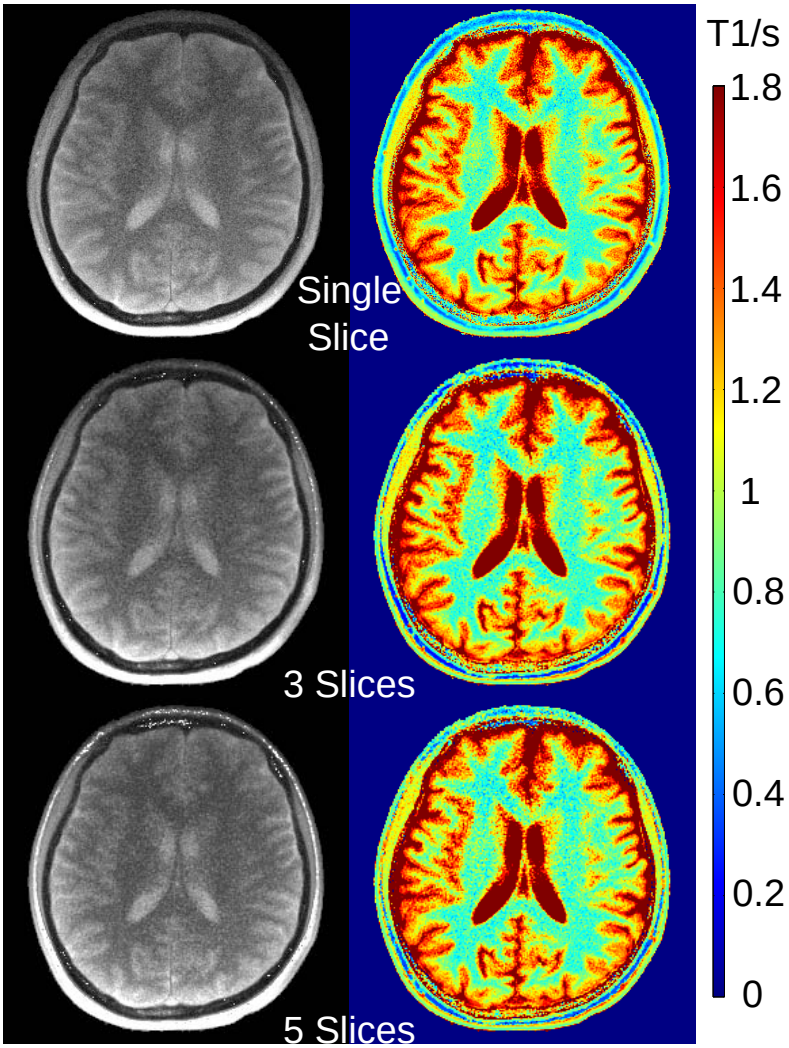

Fig. (4). Single-shot proton density and T1 maps obtained for human brain (healthy subject). (Top) Single-slice acquisition at 0.5 mm in-plane resolution, (middle) 3-slice and (bottom) 5-slice acquisition at 0.75 mm resolution (same section). For experimental details see Table **1**, numerical results are given in Table **3**.

Table 3. T1 relaxation times of the human brain, liver and kidney obtained by single-slice and multi-slice T1 mapping.

Tissue	1 Slice	3 Slices	5 Slices	Literature
Frontal WM	0.73 ± 0.11	0.73 ± 0.10	0.74 ± 0.12	0.80 – 0.88 [16]
Parietal WM	0.78 ± 0.08	0.78 ± 0.09	0.78 ± 0.08	
Frontal GM	1.36 ± 0.14	1.39 ± 0.10	1.38 ± 0.13	1.35 – 1.50 [17]
Parietal GM	1.49 ± 0.12	1.48 ± 0.11	1.48 ± 0.07	
Liver	0.68 ± 0.05	0.68 ± 0.05	0.67 ± 0.04	0.76 ± 0.15 [17]
Kidney cortex	1.30 ± 0.08	1.26 ± 0.07	1.27 ± 0.08	1.38 ± 0.10 [18]
Kidney medulla	1.75 ± 0.09	1.75 ± 0.08	1.77 ± 0.05	1.65 ± 0.09 [18]

All values (mean ± SD) are given in s. Multi-slice data refer to the same section.

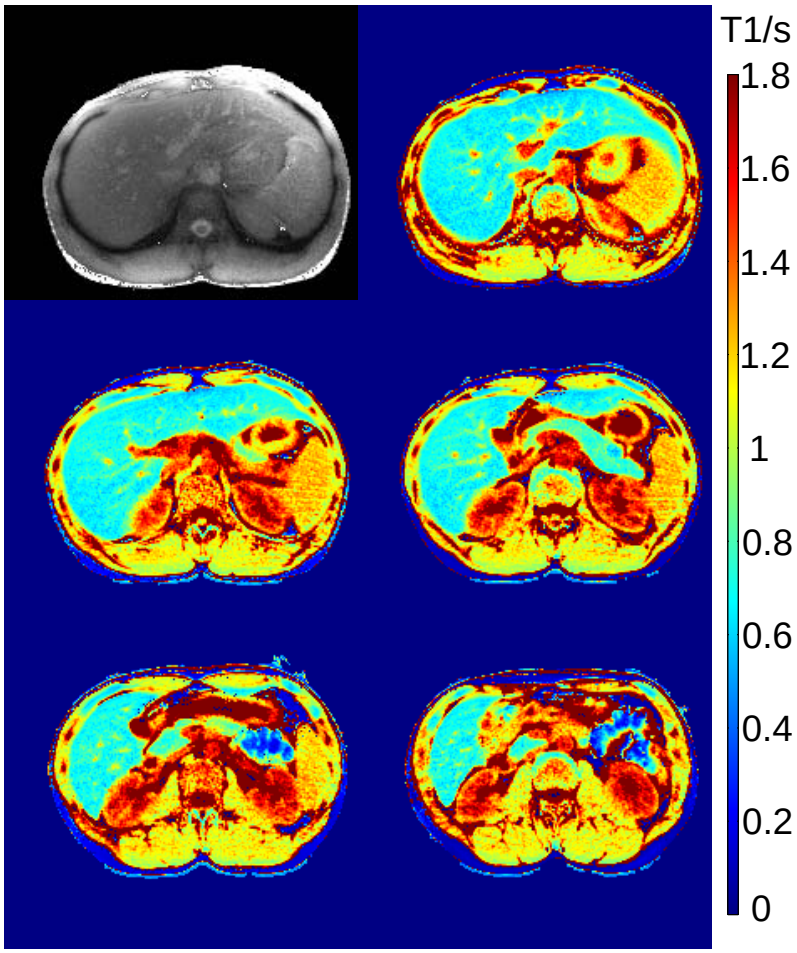

Fig. (5). (Top left) Single-shot proton density (first section) and (top right to bottom right) simultaneous multi-slice T1 maps at 1.5 mm resolution obtained for human liver (healthy subject). For experimental details see Table **1**, numerical results are given in Table **3**.

easy to implement. However, at present, a limitation is the need for offline reconstruction, although an implementation on our existing online-GPU system is under preparation.

In summary, the proposed multi-slice technique for single-shot T1 mapping and its applications to different organ systems demonstrate considerable potential, but certainly await larger clinical trials. Future developments will be extended to dynamic versions involving repetitive IR or saturation recovery FLASH sequences.

CONFLICT OF INTEREST

The authors confirm that this article content has no conflicts of interest.

ACKNOWLEDGEMENTS

Declared none.

REFERENCES

[1] Haase A. Snapshot FLASH MRI. Applications to T1, T2, and chemical-shift imaging. Magn Reson Med 1990; 13: 77-89.

[2] Ordidge RJ, Gibbs P, Chapman B, Stehling MK, Mansfield P. High-speed multislice T1 mapping using inversion-recovery echo-planar imaging. Magn Reson Med 1990; 16: 238-45.

[3] Scheffler K, Hennig J. T1 quantification with inversion recovery TrueFISP. Magn Reson Med 2001; 45: 720-3.

[4] Kellman P, Hansen MS. T1-mapping in the heart: accuracy and precision. J Cardiovasc Magn Reson 2014; 16: 2.

[5] Deichmann R, Haase A. Quantification of T1 values by Snapshot-FLASH NMR imaging. J Magn Reson 1992; 96: 608-12.

[6] Nekolla S, Gneiting T, Syha J, Deichmann R, Haase A. T1 maps by k-space reduced Snapshot-FLASH MRI. J Comput Assist Tomogr 1992; 16: 327-32.

[7] Tran-Gia J, Stäb D, Wech T, Hahn D, Köstler H. Model-based acceleration of parameter mapping (MAP) for saturation prepared radially acquired data. Magn Reson Med 2013; 70: 1524-34.

[8] Zhang S, Uecker M, Frahm J. T1 mapping in real time: Single inversion-recovery radial FLASH with nonlinear inverse reconstruction. Proc Intl Soc Magn Reson 2013; 21: 3700.

[9] Uecker M, Hohage T, Block KT, Frahm J. Image reconstruction by regularized nonlinear inversion – Joint estimation of coil sensitivities and image content. Magn Reson Med 2008; 60: 674-82.

[10] Uecker M, Zhang S, Voit D, Karaus A, Merboldt KD, Frahm J. Real-time MRI at a resolution of 20 ms. NMR Biomed 2010; 23: 986-94.

[11] Uecker M, Zhang S, Voit D, Merboldt KD, Frahm J. Real-time MRI-Recent advances using radial FLASH. Imaging Med 2012; 4: 461-76.

[12] Zhang S, Joseph AA, Voit D, *et al*. Real-time magnetic resonance imaging of cardiac function and flow – Recent progress. Quant Imaging Med Surg 2014; 4: 313-29.

[13] Zhang S, Block KT, Frahm J. Magnetic resonance imaging in real time: using radial FLASH. J Magn Reson Imaging 2010; 31: 101-9.

[14] Pruessmann KP, Weiger M, Scheidegger MB, Boesiger P. SENSE: Sensitivity encoding for fast MRI. Magn Reson Med 1999; 42: 952-62.

[15] Santyr GE, Fairbanks EJ, Kelcz F, Sorenson JA. Off-resonance spin locking for MR imaging. Magn Reson Med 1994; 32: 43-51.
[16] Liberman G, Louzoun Y, Ben Bashat D. T1 Mapping using variable flip angle SPGR data with flip angle correction. J Magn Reson Imaging, 2014; 40: 171-80.
[17] Haimerl M, Verloh N, Zeman F, *et al*. Assessment of clinical signs of liver cirrhosis using T1 mapping on Gd-EOB-DTPA-enhanced 3T MRI. PLoS One 2013; 8: e85658.
[18] Gillis KA, McComb C, Foster JE, *et al*. Inter-study reproducibility of arterial spin labelling magnetic resonance imaging for measurement of renal perfusion in healthy volunteers at 3 Tesla. BMC Nephrol 2014; 15: 23.
[19] Winkelmann S, Schaeffter T, Koehler T, Eggers H, Doessel O. An optimal radial profile order based on the golden ratio for time-resolved MRI. IEEE Trans Med Imaging 2007; 26: 68-76.
[20] Kunth M, Seiberlich N, Ehses P, Gulani V, Griswold M. Improvement of quantitative MRI using radial GRAPPA in conjunction with IR-TrueFISP. Proc Intl Soc Mag Reson Med 2010; 18: 2895.
[21] Ehses P, Seiberlich N, Ma D, *et al*. IR TrueFISP with a golden-ratio-based radial readout: Fast quantification of T1, T2 and proton density. Magn Reson Med 2013; 69: 71-81.

Received: August 28, 2014 Revised: November 17, 2014 Accepted: December 16, 2014